

Article

# Comparison of Heat Transfer Enhancement Techniques in Latent Heat Storage

William Delgado-Diaz , Anastasia Stamatiou \* , Simon Maranda, Remo Waser and Jörg Worlitschek 

Competence Center Thermal Energy Storage (CCTES), Lucerne University of Applied Sciences and Arts, 6048 Horw, Switzerland; williamorlando.delgadodiaz@hslu.ch (W.D.-D.); simon.maranda@hslu.ch (S.M.); remo.waser@hslu.ch (R.W.); joerg.worlitschek@hslu.ch (J.W.)

\* Correspondence: anastasia.stamatiou@hslu.ch

Received: 22 June 2020; Accepted: 3 August 2020; Published: 10 August 2020



**Abstract:** Latent Heat Energy Storage (LHES) using Phase Change Materials (PCM) is considered a promising Thermal Energy Storage (TES) approach as it can allow for high levels of compactness, and execution of the charging and discharging processes at defined, constant temperature levels. These inherent characteristics make LHES particularly attractive for applications that profit from high energy density or precise temperature control. Many novel, promising heat exchanger designs and concepts have emerged as a way to circumvent heat transfer limitations of LHES. However, the extensive range of experimental conditions used to characterize these technologies in literature make it difficult to directly compare them as solutions for high thermal power applications. A methodology is presented that aims to enable the comparison of LHES designs with respect to their compactness and heat transfer performance even when largely disparate experimental data are available in literature. Thus, a pair of key performance indicators (KPI),  $\Phi_{PCM}$  representing the compactness degree and NHTPC, the normalized heat transfer performance coefficient, are defined, which are minimally influenced by the utilized experimental conditions. The evaluation procedure is presented and applied on various LHES designs. The most promising designs are identified and discussed. The proposed evaluation method is expected to open new paths in the community of LHES research by allowing the leveled-ground contrast of technologies among different studies, and facilitating the evaluation and selection of the most suitable design for a specific application.

**Keywords:** heat transfer; high power; latent heat; energy storage; heat exchanger

## 1. Introduction

On the path to the integration of an ever-increasing share of variable renewable energy sources (VRES) into the current energy system, energy storage (ES) technologies play a fundamental role. Energy transformation and consumption globally account for more than 60% of the total green house gas emissions [1]. Additionally, in Switzerland and the European Union in general, over 50% of the total energy consumed is ultimately used as thermal energy for both industry and domestic applications [2,3]. Considering this, the development of thermal energy storage (TES) systems has become a priority for directly pure thermal applications and heat management systems, as well as combined electro-thermal storage initiatives, such as pumped thermal energy storage systems [4] and its potential for alternative use and flexibility for recovered waste heat from already existing sources at large scales [5].

Within the spectrum of TES technologies, Latent Heat Energy Storage (LHES) systems using Phase Change Materials (PCM) allow for thermal energy storage and release within narrow temperature differences with high energy density when compared to the sensible energy storage

(SES) approach. These characteristics ultimately allow for the implementation of TES systems with a high degree of compactness. The heat transfer performance of LHES systems is however hindered by the time-dependent nature of its charging and discharging processes. During crystallization, the heat transfer and phase change processes are thus dominated by conduction under increasing resistance imposed by the moving liquid-solid front, making them a function of the state of charge of the unit [6]. Thus, the widespread application of LHES units on processes that require high heat transfer rate and quick response time relies on the many novel promising technological approaches that have emerged as a way to bypass LHES heat transfer limitations. These technologies include plain tube and finned tube bundle configurations [7–14], carbon composites and dispersions [15–20], metal foams [21–26], macroencapsulation techniques [27–31], and addition of conductive nanoparticles [32–34], among others.

The extensive range of experimental conditions (e.g., inlet temperature and mass flow rate of heat transfer fluid, phase change temperature, size of storage unit, etc.) used to characterize these technologies in literature make it difficult to directly compare and cross-correlate various performance features. This variability makes heat transfer performance and the degree of compactness especially hard to assess without leveled Key Performance Indicators (KPI). Some KPIs have been proposed to evaluate different aspects of an LHES unit. For instance, Energy density (ED) as proposed by Romani et al. [35] provides an indication of the amount of energy stored in relationship to the volume or mass of the unit. ED allows for valuable comparison of TES technologies in terms of overall capacity and required space and material resources, but most relevantly in the case of LHES, it equally considers sensible and latent contributions. By considering the sensible part of the energy stored in the PCM, the result is dependent on the operation temperature levels on the unit and not only the materials and amounts. Alternatively, the energy efficiency ratio described by Wang et al. [36] concerns the ratio of energy required to pump the HTF through the LHES unit to the stored energy. In addition, in a similar approach, Li et al. [37] also proposed the performance analysis of a wide range of LHES operational and material parameters, as both energetic and exergetic efficiencies. Even though the previously described KPIs provide very valuable information about an LHES unit, they address particular aspects and consider mostly capacity and efficiency perspectives, but provide no indication on the rates of heat transfer and the required material to achieve it.

Directly addressing the thermal response, Gasia et al. [38] proposed various KPI for both short and long term scales: Average power, 5 min-peak-power, 5 min peak power-energy ratio (based on 5-min-peak-power over total capacity of the unit), and finally the discharge time. The set of KPIs was intended for the evaluation of four LHES units of very similar scales, operating at uniform conditions and equal PCM. Although useful while the experimental conditions and the geometry remain similar enough, they remain intrinsically connected to the current operation conditions and scale. This leads to non-representative results, especially when comparing across different studies and applications. Similarly, Guo et al. [39] consider the specific charging rate ( $\gamma$ [1/h]) and specific energy loss rate. The specific charging rate directly addresses the heat transfer performance of the unit, but it is ultimately an average power to capacity ratio, without any normalization with respect to the driving forces.

Similar analyses include, for instance, the use of the average temperature effectiveness ( $\epsilon_{avg}$ ) by Nomura et al. [40] and Krimmel et al. [41] to represent the efficiency of the heat exchange. Additionally, Nomura et al. [40] present a NHTPC ( $h_v$ ), directly addressing the heat transfer performance of the units. It considers the average heat transfer rate divided by the average temperature difference (which ultimately can be interpreted as the enthalpy flow of the HTF), with respect to the volume of PCM only in the unit. Although it directly addresses the heat transfer capability of a unit, it still remains dependent on the HTF conditions, and thus varies with different mass flow and temperature difference.

The Effectiveness-NTU Method ( $\epsilon$ -NTU) allows the calculation of the heat transfer rate and temperature profiles in a heat exchanger using the enthalpy flows, and defining a heat exchanger effectiveness based on the actual heat transfer rate over the maximum achievable by the system [42].

It has been previously used to analyze LHES systems as performed by Tay et al. [43,44] as design and sizing tool on specific designs.

The methodology presented in this paper is inspired on the previous ( $\epsilon$ -NTU) analyses and the view of LHES units as a heat exchanger core acting as boiler or condenser. It focuses on two KPIs, which represent the normalized heat transfer performance and degree of compactness of the LHES design. This new approach allows the comparison of LHES systems reported in literature in terms of their heat transfer capabilities and compactness regardless of their geometry, scale, and operation conditions. The developed KPIs are applied to several technologies reported in literature and the results of this comparison are presented and discussed. Based on the authors' knowledge, this is the first time such an extensive quantitative comparison across different LHES technologies with a focus on high power applications has been performed.

## 2. Methodology

### *Definition of Proposed KPIs*

The main focus of this study is to allow the simplified and quick evaluation of the heat transfer capabilities in a LHES unit regardless of scale and operating conditions. Achieving this goal requires the usage of the most readily available information able to represent a highly transient process through averaged properties. The methodology proposed in this study uses this information adapted around the ( $\epsilon$ -NTU) method. Two KPI are proposed representing both the heat transfer performance of a LHES unit as well as the degree of compactness and an indication of the energy density attainable by the system.

Regarding the degree of compactness, the volume fraction of the major contributor to the storage capacity of the LHES unit, PCM to total volume of the unit, ( $\Phi_{PCM}$ ) is suggested as an indicator of the energy density attainable by the system.  $\Phi_{PCM}$  provides an indication of the compactness degree attainable, but also information on the required trade-off of PCM storage volume for heat exchanger material to achieve certain heat transfer performance, and it is the ratio of PCM volume in the storage ( $V_{PCM}$ ) to the total outer volume of the unit ( $V_{TOT}$ ). See Equation (1)

$$\Phi_{PCM} = \frac{V_{PCM}}{V_{TOT}} \quad (1)$$

The total volume ( $V_{TOT}$ ) was calculated considering the geometry of the outermost layer of the unit while excluding the additional volume used for insulation. The container wall thickness as well as additional volume dedicated to manifolds (flow development) and the like were all taken into account.

From a heat exchanger perspective, an LHES unit can be regarded as a heat exchanger, the performance of which is defined by a static heat sink or source, or an analog case of a heat exchanger operating as a boiler or condenser. The average NTU ( $NTU_{avg}$ ) represents the added effects of the heat exchanger tubes and growing layer of solid through the discharge process. It is defined as the ratio of the heat transfer rate capacity of the heat exchanger (product of the overall heat transfer coefficient ( $U$ ) and the heat exchange surface ( $A$ )), and the heat capacity rate of the HTF ( $\dot{m}_{HTF} \cdot c_{p,HTF}$ ) [45].

Additionally, the average NTU can be easily estimated as it is directly related to the average effectiveness ( $\epsilon_{avg}$ ) of the heat exchange, and under the assumptions of a phase change, similarly to boiler/condenser operation, the heat exchanger effectiveness relations can be simplified [45] as described in Equation (2):

$$NTU_{avg} = \frac{U \cdot A}{\dot{m}_{HTF} \cdot c_{p,HTF}} = -\ln(1 - \epsilon_{avg}) \quad (2)$$

This equation can be rearranged and divided by the total volume  $V_{TOT}$  to calculate the normalized heat transfer performance coefficient (NHTPC) as shown below in Equation (3):

$$\text{NHTPC} = \frac{U \cdot A}{V_{TOT}} = \frac{-\ln(1 - \varepsilon_{avg}) \cdot \dot{m}_{HTF} \cdot c_{p,HTF}}{V_{TOT}} \quad (3)$$

Thus, the proposed KPI on the heat transfer side, NHTPC, can be seen as the product of the overall heat transfer coefficient ( $U$ ) and the heat exchange surface ( $A$ ) normalized by the total volume of the LHES unit ( $V_{TOT}$ ). Considering the transient nature of the solidification process due to the increasing resistance and changing surface, it is useful to express an average  $U \cdot A$  for the whole process. Dividing this product by the total volume of the LHES unit ( $V_{TOT}$ ) excluding insulation enables comparison of the heat transfer behavior regardless of the final dimensions, operation conditions, and overall scale.

Where  $\varepsilon_{avg}$  represents the average heat exchanger effectiveness during discharge,  $\dot{m}_{HTF}$  and  $c_{p,HTF}$ , the mass flow rate and specific heat capacity of the HTF, respectively, and finally  $V_{TOT}$  the total outer volume of the container without considering any insulation.

In this case, the effectiveness of the heat transfer ( $\varepsilon_{avg}$ ) is defined by the relation of the actual average (over the discharge time) temperature difference between inlet ( $\overline{T_{HTF,In}}$ ) and outlet ( $\overline{T_{HTF,Out}}$ ), and the theoretical maximum temperature difference achievable, with respect to the phase change temperature ( $T_{PC}$ ) as shown in Equation (4) [43,45].

The  $T_{PC}$  values were reported by the individual studies, and are usually obtained through differential scanning calorimetry (DSC) measurements:

$$\varepsilon_{avg} = \frac{\overline{T_{HTF,In}} - \overline{T_{HTF,Out}}}{\overline{T_{HTF,In}} - T_{PC}} \quad (4)$$

This relation allows access to the average product “ $U \cdot A$ ”, or the average heat rate capacity of the heat exchange geometry in the core of the unit. This quantity can be considered independent of the operation conditions, but remains an intrinsic characteristic of the heat exchanger geometry, design, and material combination (PCM and heat exchanger materials).

During the solidification process, the conductive resistance between the HTF and the solidifying (liquid) PCM increases as solid PCM builds up around the HEX structure surface. This also generates a changing solid–liquid PCM heat transfer surface throughout the process. With this in mind, it can be especially handy to consider the product  $U \cdot A$  averaged through time, since both the heat transfer surface, and heat transfer coefficient, vary throughout the discharge process with the state of charge of the unit.

Even though the main required information pertaining to the geometry, materials, and amounts are uniformly available, how and which experimental results are readily displayed in literature remains very dependent on the authors and the focus of the studies. Some additional considerations to the definition of the pair of the previously discussed KPIs are suggested for an even representation with the proposed KPIs:

The average HTF outlet temperature ( $\overline{T_{HTF,Out}}$ ) was preferably estimated by fitting a polynomial function to the reported data and calculating a mean function value between the beginning of the discharge process up to an arbitrary point. For practical purposes, and considering that once a high degree of solidification is attained the power sharply decreases, a 90% solidification or melting is considered as a standard for a completed process and thus is defined as discharge time ( $t_{Disch}$ ).

For the few cases in which outlet temperature or power profiles were not provided,  $\overline{T_{HTF,Out}}$  can be approximated as shown in Equation (5) derived from the simplified steady-flow thermal energy equation [45]:

$$\overline{T_{HTF,Out}} = \overline{T_{HTF,In}} + \frac{\dot{Q}_{avg}}{\dot{m}_{HTF} \cdot c_{p,HTF}} \quad (5)$$

Knowing  $t_{Disch}$  conveniently allows for indirectly representing the average output power-to-capacity ratio as it represents the inverse of the time required to achieve a certain amount of PCM solidification, and thus the average discharge power ( $\dot{Q}_{avg}$ ) can be approximated using Equation (6) [46] and the energy balance based on material properties and temperature levels:

$$\frac{\dot{Q}_{avg}}{E_{st,90}} = \frac{1}{t_{Disch}} \quad (6)$$

The energy associated with the defined standard degree of solidification ( $E_{st,90}$ ) is estimated assuming the complete contribution of the sensible heat from container ( $m_{Cont} \cdot c_{p,Cont}$ ) and heat exchanger materials ( $m_{HEX} \cdot c_{p,HEX}$ ) and PCM ( $m_{PCM} \cdot c_{p,PCM}$ ) from the initial temperature of the unit  $T_{init}$  up to the phase change temperature of the PCM  $T_{PC}$  in addition, to 90% of the latent contribution from the PCM, as shown in Equation (7):

$$E_{st,90} = (m_{HEX} \cdot c_{p,HEX} + m_{Cont} \cdot c_{p,Cont} + m_{PCM} \cdot c_{p,PCM}) \cdot (T_{init} - T_{PC}) + (90\% \cdot m_{PCM} \cdot \Delta h_{PC}) \quad (7)$$

Using these considerations and assumptions allows for the calculation of the proposed NHTPC with minimal representative information. The results of the preliminary analysis are shown and discussed subdivided in similarity classes, with a specific focus on the heat transfer performance and the potential of the different approaches for applications that require high power LHES systems.

In summary,  $\Phi_{PCM}$  represents the ratio of main energy storage material to the total volume of the unit, excluding insulation. It provides a general idea on the compactness degree of the system and energy density potential by remaining independent of the temperature levels. Additionally, it can be regarded as a representation of the required HEX material to attain a certain heat transfer performance. It only requires the overall dimensions of the unit and the total amount of PCM inside for its calculation.

NHTPC represents the average heat transfer performance of an LHES unit regardless of the operation conditions (HTF flowrate and temperature levels) used by the authors of the different studies but remaining an intrinsic characteristics of the heat exchange structure geometry, and material combinations (PCM, HEX, container, etc.). The calculation requires, in principle, information on both inlet and outlet temperatures on the unit and material properties of PCM and the different components (HEX and container). Temperature profiles are preferably used to estimate directly the average temperatures by using fitting techniques, mean function values, and the previously defined  $E_{st,90}$  from the energy balance. Alternatively, if this information is not presented directly, average discharge power or the discharge time can be used to compute close approximations, as shown in Equations (5)–(7).

### 3. Results and Discussion

Only the studies that provided sufficient information to perform the calculations with minimal assumptions are shown and discussed in this study. The analysis of the different cases is presented subdivided in four subclasses, namely, finned tube bundle heat exchanger structures, composites of different natures as Thermal Conductivity Enhancers (TCE), macro encapsulation based systems, and experiments using automotive heat exchanger structures and capillary tube bundles.

#### 3.1. Robustness Testing

In order to corroborate the relative independence of the proposed KPIs with regard to the operation conditions and scale of the LHES unit under scrutiny, a sensitivity analysis incorporating results from a sample of studies in which different inlet temperatures ( $T_{HTF,In}$ ) and HTF mass flow rate ( $\dot{m}_{HTF}$ ) were used.

The influence of the inlet temperature on the final NHTPC was examined using data from Waser et al. [7] and considering three  $T_{HTF,In}$  levels between 15 °C and 40 °C in both a tube bundle

(Unit 1) with  $0.02\text{ m}^3$  (20 kg of PCM,  $\text{CH}_3\text{COONa}\cdot 3\text{H}_2\text{O}$ ), and the equivalent finned tube bundle (Unit 2) under a constant 360 kg/h of flowing water as HTF. The mass flow rate effect was considered using data from two different sources and consistent temperature levels. On a larger scale, the data gathered by Zauner et al. [47] for a storage of  $0.4\text{ m}^3$  total outer volume (170 kg of PCM, HDPE) operating with thermal oil (Marlotherm SH) as HTF between 2088 kg/h up to 6984 kg/h (Unit 3) was used. On the smaller side, the unit shown by Amagour et al. [13] is considered (Unit 4) with a total outer volume of  $0.009\text{ m}^3$  (2.3 kg of PCM, organic blend) with water as HTF and flow rates ranging between 24 kg/h and 62 kg/h.

Figure 1 shows the obtained results for the analysis of the ability of the KPIs to describe system performance independently of experimental conditions.

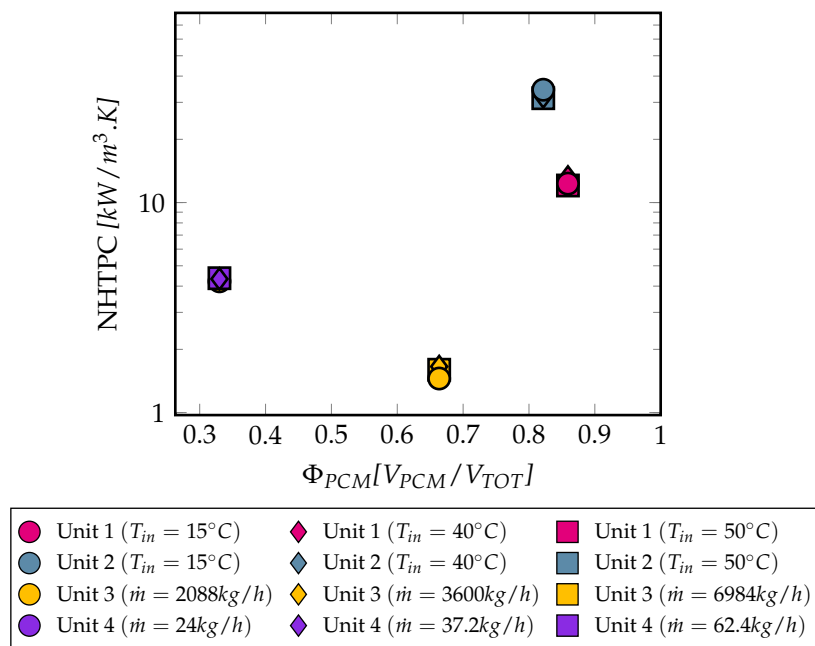


**Figure 1.** Sensitivity analysis. Calculated NHTPC vs.  $\Phi_{PCM}$  at different temperature levels and HTF mass flow rates in logarithmic scale.

The tight spread of the final results for all four cases corroborates the relative independence of the proposed KPI to the operation conditions. Even though small variations were found for the different experiments, an average coefficient of variation (defined as the standard deviation over the average value) of less than 6% was calculated for every case, which is considered satisfactory for the purpose of this study.

### 3.2. Finned Tube Bundles

Finned Tube Bundle (FTB) geometries are the most widely studied Heat Exchanger (HEX) configuration for LHES applications. They consist of fixed-fin geometries, of different topologies and configurations, generally protruding from the tubes used to carry the HTF, into the PCM mass. Highly conductive metals such as copper and aluminum are the most commonly used. The disposition of the fins, packing fraction, thickness, and amount determine the performance of a finned tube bundle.

The selection of analyzed studies which addressed the addition of fins to a tube bundle (TB) heat exchanger geometry to enhance the heat transfer rates of a LHES unit is summarized in Table 1. It includes reference numbers, notation, some descriptive information, and a representative picture or scheme of the discussed units. All additional data required for the calculation of NHTPC are presented in Table A1. The outer volumes of the units  $V_{TOT}$ , including the container tank surrounding the TB or FTB (and additional manifolds if required) without considering any insulation, were for the most part explicitly reported along with container material and properties. In the cases where information

was missing in this regard, it could be approximated from additional reported geometrical parameters and conservative assumptions. Figure 2 presents the estimated performance indicators. Experiments performed in the framework of the same study with different geometries are indicated with the same letter but different numbering.

**Table 1.** References pertaining to tube bundles (TB) and finned tube bundles (FTB).

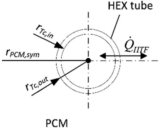
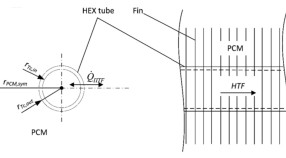
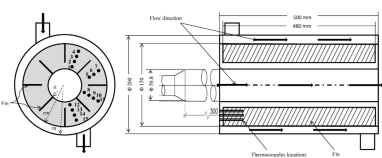
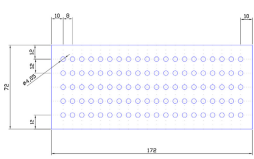
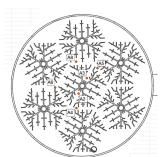
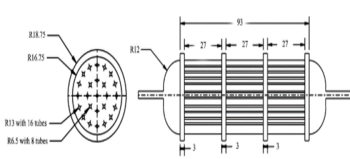
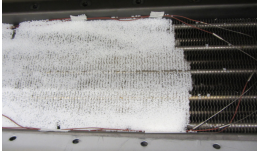
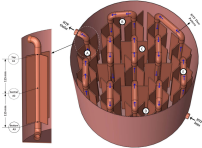
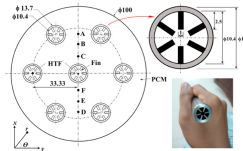
Type	$T_{PC}$ [°C]	$V_{TOT}$ [m <sup>3</sup> ]	$\dot{m}_{HTF}$ [kg h <sup>-1</sup> ]	$c_{p,HTF}$ [kJ/(kg · K)]	Geometry	Ref.
TB (A.1)	58	$2.0 \times 10^{-2}$	$3.6 \times 10^2$	4.18		[7]
FTB (A.2)	58	$2.0 \times 10^{-2}$	$3.6 \times 10^2$	4.18		[7]
TB (B.1)	35	$9.3 \times 10^{-4}$	$4.0 \times 10^2$	4.18		[48]
FTB (B.2)	35	$9.3 \times 10^{-4}$	$4.0 \times 10^2$	4.18		[48]
Triplex FTB(C)	82	$1.6 \times 10^{-2}$	$2.4 \times 10^2$	4.18		[9]
FTB (D.1)	94	$3.4 \times 10^{-3}$	$2.2 \times 10^3$	4.06		[14]
FTB (E)	305	$3.5 \times 10^{-1}$	$8.1 \times 10^3$	2.30		[10]
FTB (F)	142	$8.7 \times 10^{-2}$	$2.4 \times 10^2$	2.49		[8]

Table 1. Cont.

Type	$T_{PC}$ [°C]	$V_{TOT}$ [m <sup>3</sup> ]	$\dot{m}_{HTF}$ [kg h <sup>-1</sup> ]	$c_{p,HTF}$ [kJ/(kg · K)]	Geometry	Ref.
FTB (G)	125	$3.9 \times 10^{-1}$	$1.5 \times 10^3$	2.03		[47]
FTB (H)	53	$8.7 \times 10^{-3}$	$2.4 \times 10^1$	4.18		[13]
FTB (I)	42	$6.1 \times 10^{-2}$	$1.8 \times 10^2$	4.18		[49]
FTB (J)	169	$6.5 \times 10^{-3}$	$3.5 \times 10^2$	3.10		[12]

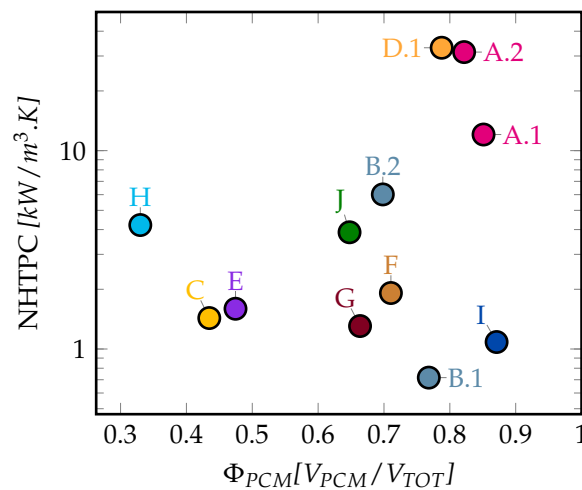


Figure 2. Calculated NHTPC vs.  $\Phi_{PCM}$  for the references concerning tube bundles (TB) and finned tube bundles (FTB) in LHES unit configurations in logarithmic scale.

The most commonly found arrangements pertain fixed fins embedded in the PCM bulk, oriented perpendicularly (A.2, B.1, D, G, H) or longitudinally (C, E, F, I, J) to the HTF flow inside the tubes. Some interesting alternative variations see longitudinal fins used such as in triplex heat exchanger configurations by Al-Abidi et al. [9] (C), complex geometries to fit specific applications by Laing et al. [10] (E) or even fixed on the side of the flowing HTF, as presented by Raul et al. [12] (J). Regarding performance, the study carried out by Waser et al. [7] provided data for a finned copper tube bundle (A.2) and additional in-house data from the same study was used for the analog plain tube bundle (A.1). The addition of aluminum fins traded an additional 3% of PCM volume fraction for a

significant discharge time reduction of around 50% and a total threefold improvement in the calculated NHTPC. However, it is necessary to highlight the performance of the tube bundle structure (A.1) as it exceeds most of the FTB designs. Taking the unit used by Khan et al. [49] (I) as comparison point, the sheer difference in heat transfer surface could explain this behavior. Even though A.1 presents no fins, the heat transfer surface to volume ratio of unit A.1 is over two times higher ( $63 \text{ m}^2/\text{m}^3$ ) than that of unit I ( $27 \text{ m}^2/\text{m}^3$ ).

In a similar comparison approach, Medrano et al. [48] (B.2) achieved a sevenfold increase (when compared to B.1) in heat transfer performance by trading an approximate 7% of PCM volume to accommodate circular radial fins.

The FTB unit presented by Shon et al. [14] (D.1) attained the higher performance in this case with an additional 4% of the total volume dedicated to the analog copper finned tubes than the FTB unit investigated by Waser et al. [7]. The heat exchange structure with a higher packing fraction could explain the differences in performance.

In the case of Amagour et al. [13] (H), it is interesting to note that around 65% of the total LHES unit volume was dedicated to heat exchange elements as well as additional empty space above the heat exchanger. It directly affects the overall energy density of the unit with around  $29 \text{ kWh}/\text{m}^3$ , but achieves a thermal response around the average for the category. This is evidence of the intricacies of the container, heat exchanger design, and chosen materials. A high share of heat exchanger material, or consequently a low PCM fraction, does not necessarily translate into improved heat transfer behavior. A similar situation was found on some other cases leading to a low  $\Phi_{PCM}$  was caused by a large volume occupied by the HTF, and additional head space in the units which could potentially be optimized.

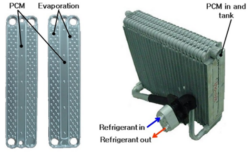
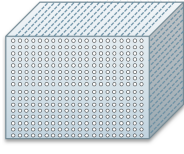
### 3.3. Automotive Heat Exchangers and Polymer Based Capillary Scale Tube Bundles

This entire subsection is dedicated to particularly interesting systems as they are in principle extreme variations of finned and simple tube bundles. On one hand, Automotive HEX (AHEX), conceived from the idea of finned tubes for gas-to-liquid heat exchange, are mass produced on a wide variety of configurations usually completely made out of braced aluminum and seek to maximize the heat transfer surface. On the other hand, without additional material, very large heat transfer surfaces can be achieved by driving the diameter of a tube bundle to the capillary scale (below 5 mm). Additionally, the consequent thin walls produced at this scale minimize the influence of the material conductivity, opening the door to the utilization of polymers for a wide range of applications when temperature levels allow. These systems will be finally referred to as capillary tube bundles (CTB). Table 2 gathers the notation and representative schemes of the studies treated in this section. All additional data required for the calculation of NHTPC are presented in Table A1. The outer volumes of the units  $V_{TOT}$ , including the container tank surrounding the HEX without considering any insulation, were for the most part explicitly reported in the different studies along with container material and properties. In the cases where information was missing in this regard, it could be approximated from additional reported geometrical parameters and conservative assumptions.

The summarized KPIs are portrayed in Figure 3. Experiments performed in the framework of the same study with different geometries are indicated with the same letter but different numbering.

Medrano et al. [48] experimented with an AHEX unit embedded in PCM (B.4), and compared it to other common LHES approaches and it achieved an impressive NHTPC, several times higher than the next best performance within the same study, the graphite matrix enhanced tube-and-shell (B.3) unit previously discussed. This effect might be explained mainly by the sheer mass of heat exchanger material in the unit rather than the heat exchanger design as it presents a relatively low performance in both heat transfer and compactness when compared to other AHEX-based units.

**Table 2.** References pertaining to AHEX and CTB based units.

Type	$T_{PC} [^{\circ}C]$	$V_{TOT} [m^3]$	$\dot{m}_{HTF} [kg\ h^{-1}]$	$c_{p,HTF} [kJ/(kg \cdot K)]$	Geometry	Ref.
AHEX (B.4)	35	$4.4 \times 10^{-3}$	$4.00 \times 10^2$	4.18		[48]
AHEX (S)	4	$4.1 \times 10^{-3}$	$5.34 \times 10^2$	1.01		[50]
AHEX(T)	69.3	$3.3 \times 10^{-3}$	$7.13 \times 10^2$	3.95		[51]
AHEX(D.2)	93.8	$1.9 \times 10^{-3}$	$2.21 \times 10^3$	4.06		[14]
CTB (U)	30	1.0	$3.60 \times 10^3$	4.18		[52]
CTB (V)	29	$8.5 \times 10^{-1}$	$1.38 \times 10^3$	4.18		[53]
CTB (W)	28.5	1.5	$3.15 \times 10^3$	4.18		[54]

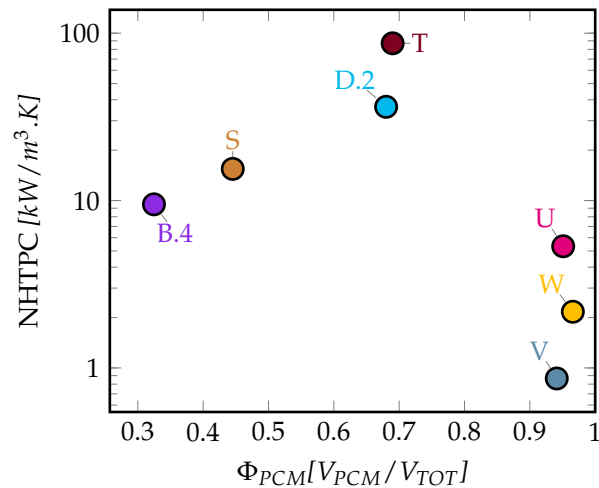


**Figure 3.** Calculated NHTPC vs.  $\Phi_{PCM}$  for the references concerning AHEX and CTB in LHES unit configurations in logarithmic scale.

A similar situation was discussed in the study performed by Shon et al. [14] their initial experiments were performed using a stock automotive HEX immersed in PCM (D.2). Based on their results, an FTB design with a higher capacity was produced and is discussed in Section 3.2 (D.1). Interestingly, their goal was achieved as their FTB custom design (33  $\text{kW}/\text{m}^3 \cdot \text{K}$ ) effectively matched the thermal performance of the AHEX-based unit (36  $\text{kW}/\text{m}^3 \cdot \text{K}$ ). Their design variations, however, required an additional sacrifice of 10% PCM volume fraction. A second iteration of an analog system for a diesel based system, explored by Park et al. [51] (T), produced a custom heat exchanger with an analog flat pipe and fin configuration, and produced the highest NHTPC reported, reaching around 85  $\text{kW}/\text{m}^3 \cdot \text{K}$  with a similar PCM volume fraction as its predecessor. The LHES unit proposed by Lee et al. [50] (S) constitutes a particular example of how LHES capacity and power are tailored for specific applications. The high performance parameter calculated and the significantly low PCM volume fraction were adjusted to the envisioned application requirements. The unit was manufactured to produce high cooling power for very short periods of time while the car is idle on a red light, as the LHES unit is part of an automotive HVAC system, and is thus adapted to be used with two HTF systems, coolant loops and pure air convection.

These are good examples of the potential of AHEX as highly optimized systems readily available at industrial manufacturing scales in a broad variety of configurations that, although envisioned for a different application, could widen the areas of implementation of an already existing product.

When looking at polymer CTBs, their average performance does not deviate much from the results seen for FTB. They are polymer based and large heat exchange surfaces are achievable while requiring very low volume within the unit, in the order of 90% PCM fraction or more. Helm et al. produced a prototype [53] (V) and posterior improvement [54] (W) as part of a solar heating and cooling system. The heat exchange structure based on polypropylene capillary tubes in the order of 4.3 mm outer diameter was used in both cases and not only its performance, but also its durability, were put to the test in system level experiments and cycling tests.

Similarly, Hejcik et al. [52] (U) presents a special case, studying the use of polypropylene hollow fibers, capillary tubes in the order of 0.8 mm outer diameter as tube bundle arrangements embedded in PCM within a modeling study. The reported performance was calculated based on the simulations carried out by the authors and the PCM volume fraction was calculated based on the model domain used which included only a PCM mass and the hollow fiber bundle. The potential of hollow fiber bundles and, in general, polymer capillary scale systems becomes discernible when contemplating that thermal performances comparable to FTB configurations are attainable using basic geometries that occupy a minimal share of the volume.

Even though the heat transfer performance seems adequate from a KPI perspective, it is necessary to clarify that although a quick discharge can be achieved with CTB based systems, they require special attention in their design as achieving a stable temperature output window requires low mass flow rates, long tubes, or systems in series. The added frictional effects of the HTF flow at low inner diameter conditions must be considered during the optimization to avoid excessive pumping power requirements and affecting the effectiveness of the system.

### 3.4. Composites

The use of highly conductive materials to increase the performance of PCM as Thermal Conductivity Enhancements (TCE) has been widely studied. The general goal of this kind of TCE is to allow the creation of a conductive network through the PCM mass and enhance overall conduction in both melting and solidification processes. Table 3 shows the notation and representative figures of the studies considered in this subsection. All additional data required for the calculation of NHTPC are presented in Table A1. The outer volumes of the units  $V_{TOT}$ , including the container tank surrounding the HEX (and additional manifolds if required) without considering any insulation, were for the most part explicitly reported in the different studies along with container material and properties. In the cases where information was missing in this regard, it could be approximated from additional reported geometrical parameters and conservative assumptions.

**Table 3.** References pertaining to carbon based techniques and metal foams as TCE.

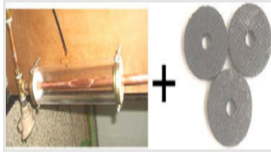
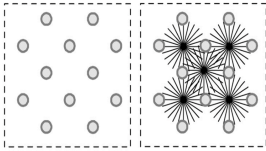
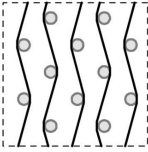
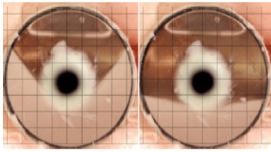
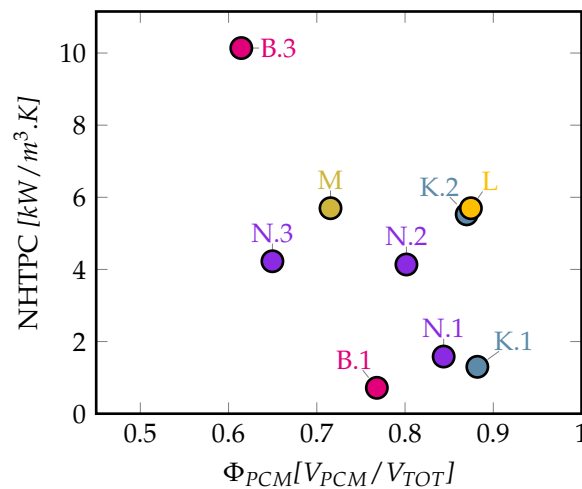
Type	$T_{PC}$ [°C]	$V_{TOT}$ [m <sup>3</sup> ]	$\dot{m}_{HTF}$ [kg h <sup>-1</sup> ]	$c_{p,HTF}$ [kJ/(kg · K)]	Geometry	Ref.
Graphite matrix (B.3)	35	$9.3 \times 10^{-4}$	400	4.18		[48]
TB (K.1); Carbon brushes (K.2)	49	$2.0 \times 10^{-2}$	32.6	4.18		[55]
Carbon cloth (L)	49	$2.0 \times 10^{-2}$	32.6	4.18		[19]
Graphite matrix (M)	53	$1.6 \times 10^{-2}$	30	4.18		[16]
TB (N.1); 95% FP (N.2); 77% FP (N.3)	58	$6.2 \times 10^{-4}$	8.14	1.01		[22]

Figure 4 summarizes the performance results of carbon and metal based TCE in different configurations, such as carbon dispersions and composites of various forms, and metal foams of different amounts of pores per inch. Each subcategory will be further discussed separately.



**Figure 4.** Calculated NHTPC vs.  $\Phi_{PCM}$  for the references concerning carbon based structures and metal foams as TCE in LHES unit configurations.

#### 3.4.1. Metal Foam Based Composites

Across the metal foams (MF) considered as TCE options for LHES systems, the most widely studied are aluminum [21,22], copper [23–25], and nickel [26] foams.

For instance, Atal et al. [22] considered aluminum foams of different porosities (N.2, N.3) on a shell and tube arrangement and achieved reductions in discharge time of up to 63% and a proportional increase in its heat transfer performance when compared to the case with only PCM (N.1). However, only a marginal increase in performance is observed with decreasing metal foam porosity (FP) (and consequently PCM volume fraction) as shown in Figure 4. An ultimate difference of around 15% additional PCM volume fraction is sacrificed to accommodate the lower porosity foam but little to no effect is shown in terms of heat transfer enhancement. Additionally, the energy density of the system is heavily affected, decreasing from 112 kWh/m<sup>3</sup> in the case of pure PCM (N.1), to 108 kWh/m<sup>3</sup> for the 95% porosity foam (N.2) and finally 94 kWh/m<sup>3</sup> in the case of the 77% porosity foam (N.3). It becomes clear that the energy density trade-off when accommodating the higher porosity foam (N.2) is worth it in terms of performance, but, once a sufficient highly conductive network is created, there is no substantial enhancement in increasing the amount of metal in the unit.

Lazzarin et al. [21] also studied the effect of aluminum foams with slightly different porosities and number of pores per inch (PPI) achieving in the best case a reduction of around 90% on the solidification time. In a similar way, Mancin et al. [23] used copper foams of increasing PPI and attained a reduction in charging time of around 27%. Similarly, Xiao et al. [24] used copper and nickel foams of different amounts of PPI to improve PCM conductivity. From the measurements performed by the authors, a great improvement is evident for all cases when compared to the original 0.305 W/m·K. For instance, the copper foams embedded in the PCM produced conductivities of 5 W/m·K and 16 W/m·K for 97% and 88.9% porosity samples, respectively.

The latter examples, although worth mentioning, are not shown in this study since their experimental setup was not conceived as LHES units working with a heat transfer fluid and thus it was not possible to accurately calculate the proposed KPIs without inaccurate assumptions. Similarly, a major share of the considered references pertaining the use of metallic foams concerned effective thermal conductivity measurements, and experimental setups focused towards electronic heat management strategies. In order to compare in terms of the NHTPC methodology, either more

experimental work or validated models that place these materials in a LHES unit configuration are necessary to further study and evaluate their potential.

### 3.4.2. Carbon-Based Composites

Among the considered references, several of them contained some form of carbon based TCE, in the form of expanded graphite composites and dispersions [15,16,20,48], carbon fiber (CF) [17], carbon foam [18], and even carbon fiber cloth (CC) [19].

Within the selected units, Medrano et al. [48] proposed the highest performance of the carbon based enhancements by placing an expanded graphite and PCM composite in a double pipe heat exchanger configuration (B.3) and compared it to a direct analog unit containing only PCM (B.1) discussed in Section 3.2. The addition of the graphite matrix required the trade of 15% in PCM volume fraction but achieved a seventeen fold increase in terms of NHTPC.

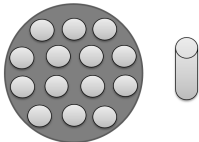
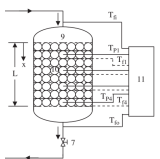
Fukai et al. [19,55] used carbon fiber brushes [55] (K.2) and carbon fiber cloth [19] (L) threaded around a copper tube bundle structure (K.1). Interestingly, both enhancements, under the same experimental conditions, reduced the discharge time by up to 45% by trading a minor share of the volume to accommodate the brushes [55] (K.2) and carbon cloth [19] (L) in both cases. Wu et al. [16] (M) produced a similar performance using shape stabilized 75:25 PCM and expanded graphite composite with a copper tube bundle configuration as heat transfer elements but required an additional 17% PCM volume fraction to achieve it.

### 3.5. Macro-Encapsulation Solutions

The considered references pertaining macro encapsulation techniques include both high and low temperature applications. The considered examples are shown in Table 4. All additional data required for the calculation of NHTPC are presented in Table A1. The outer volumes of the units  $V_{TOT}$ , including the container tank surrounding the bed of capsules (and additional manifolds if required) without considering any insulation, were for the most part explicitly reported in the different studies along with container material and properties. In the cases where information was missing in this regard, it could be approximated from additional reported geometrical parameters and conservative assumptions. The results are available in Figure 5.

Ma et al. [27] (O) and Wickramaratne et al. [28] (P) both presented LHES units using stainless steel encapsulation methods for high temperature applications on a range of temperatures around 550 °C. Even though the systems are relatively similar, the difference in performance could be explained in part by the fact that Ma et al. [27] (O) uses Al:Si alloy as PCM and Wickramaratne et al. [28] (P) proposed a eutectic salt mixture. This means that, besides having a much larger PCM phase change enthalpy (432 kJ/kg), in the first case, the most common drawback associated with LHES is minimized by the high PCM thermal conductivity in both phases. This ultimately translates into higher average power, and it is taken into account in the NHTPC, as the average outlet HTF temperature is much closer to the phase change temperature.

**Table 4.** References pertaining to macro encapsulation techniques.

Type	$T_{PC}$ [°C]	$V_{TOT}$ [m <sup>3</sup> ]	$\dot{m}_{HTF}$ [kg h <sup>-1</sup> ]	$c_{p,HTF}$ [kJ/(kg · K)]	Geometry	Ref.
ME (O)	577	$4.2 \times 10^{-3}$	19.8	1.10		[27]
ME (P)	515	$1.3 \times 10^{-2}$	70.5	1.07		[28]
ME (Q)	60	$4.7 \times 10^{-2}$	120	4.18		[30]
Pouch (R.1), Sphere (R.2)	58	$2.7 \times 10^{-1}$	900	4.18		[31]

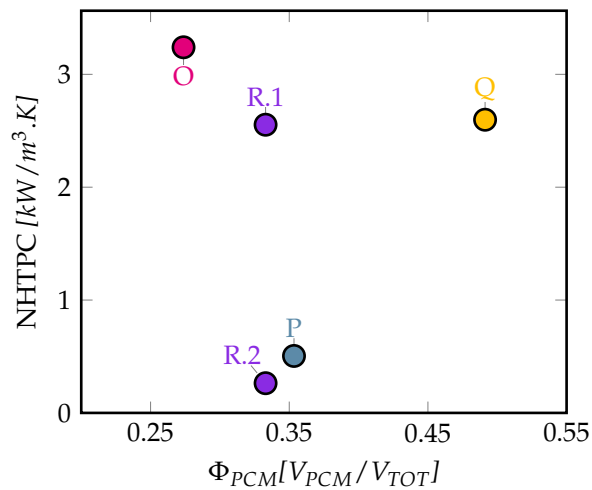


**Figure 5.** Calculated NHTPC vs.  $\Phi_{PCM}$  for the references concerning macro encapsulation techniques in LHES unit configurations.

Park et al. [31] presented flexible (Polyethylene, Nylon, Aluminum, and PET) laminated pouches (R.1) as the encapsulation method and compared them to 3D CFD modeled spherical equivalents (R.2). The flexible pouches decreased the discharge time of the system by 62% when compared to the simulated spherical containers, and is reflected on a fivefold increase in its NHTPC while retaining the same PCM fraction in the unit. This is a clear illustration of the importance of the design of the encapsulation structure in the overall heat transfer surface of the system.

Similarly, Nallusamy et al. [30] (Q) showed the highest NHTPC and PCM fraction combination calculated using HDPE spheres in a packed bed configuration.

#### 4. Discussion

Data on the geometry, thermal properties, and performance under specific conditions of a wide range of technological approaches to LHES were gathered and used to estimate NHTPC and PCM volumetric fractions. Figure 6 summarizes the LHES units in each category to enable comparison of performance across all technologies.

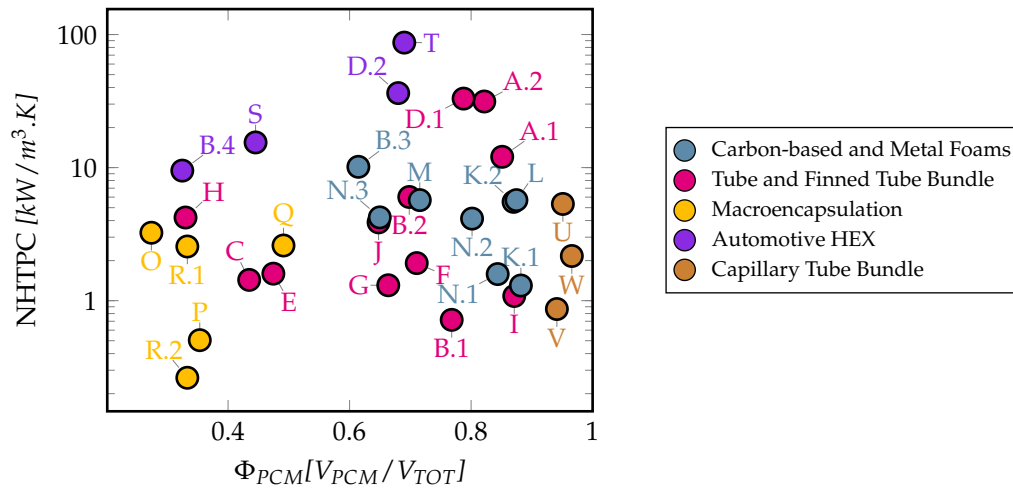


Figure 6. NHTPC vs.  $\Phi_{PCM}$  for all units in each category in logarithmic scale.

Considering the overall trends when looking at the calculated KPIs, some general observations can be drawn:

- Finned tube bundles showed a wide range of performance, and volumetric fractions of PCM. The difference among the heat exchanger structures ranged mainly on terms of tube bundle geometry and fin density. If designed properly, they have a very high potential both in terms of heat transfer and resulting capacities.
- AHES based units showed the highest average performance parameters across all technologies. This coupled with the advantages of mass production, potential for modularity, and variety of configurations makes them interesting for further study. Long-term stability and issues with flexibility of existing designs will have to be addressed before they are proposed for implementation in commercial products.
- Additionally, CTBs showed the potential to attain performances comparable to average performing finned tube bundle geometries while using a minimal share of the volume in a unit. However, the quality of the outlet temperature stability and round trip efficiency due to required pumping power at low diameters, as well as particularities regarding material compatibility and consequential limited temperature range, persist as some of the challenges for their implementation.
- Metallic foams and carbon-based TCE of all forms showed promising potential and further experimentation on optimized LHES unit structures, or simulations are required to properly assess their thermal performance.
- In contrast, among all the categories, the macroencapsulation techniques considered showed the lowest average NHTPC and  $\Phi_{PCM}$  pairs. However, the studied units were not conceived or optimized for high power applications and used relatively large capsules with a generic geometry. A large room for improvement remains untapped regarding the optimization of capsule shape and size to enhance both heat transfer performance and compactness.

#### KPI Comparison

Considering the many already available KPI for LHES systems, Table 5 compiles some of the most relevant KPIs concerning heat transfer performance and compactness degree, as well as the

pair presented in this study for three systems at different experimental conditions. Even though the considered KPIs are not intended to represent the same phenomena or were conceived with the same objectives, it is still interesting to see how they vary with experimental conditions and how they compare among each other.

Similarly to the robustness testing section, Units 2, 3, and 4 are used as representative systems, with varying inlet temperature, mass flow rate, and overall size, with the intent to analyze how the KPIs change accordingly.

**Table 5.** Comparison of different KPIs for LHES.

KPI	Unit 2 ( $T_{in}, 15^{\circ}\text{C}$ )	Unit 2 ( $T_{in}, 40^{\circ}\text{C}$ )	Unit 3 ( $\dot{m}$ , 2088 kg/h)	Unit 3 ( $\dot{m}$ , 6984 kg/h)	Unit 4 ( $\dot{m}$ , 24 kg/h)	Unit 4 ( $\dot{m}$ , 62.4 kg/h)
Energy Stored [kWh]	2.10	1.70	18.77	18.77	0.23	0.24
Energy Density [kW/m <sup>3</sup> ·K]	105.16	85.23	47.93	47.93	26.19	27.23
NHTPC [kW/m <sup>3</sup> ·K]	31.39	31.81	1.60	1.56	4.22	4.36
$\Phi_{PCM}$	0.83	0.83	0.66	0.66	0.33	0.33
$t_{Disch}$ [h]	0.15	0.28	1.75	1.20	0.28	0.22
$\dot{Q}_{avg}$ [kW]	9.37	4.96	7.90	11.52	0.63	0.80
5min-Peak Power [kW]	16.37	8.67	23.25	35.69	0.86	1.51
5m-P.Power-Energy sto.[1/h]	7.78	5.09	1.24	1.90	3.80	6.40
$\gamma$ [1/h]	4.46	2.91	0.42	0.61	2.79	3.40
$\varepsilon_{avg}$	0.77	0.78	0.41	0.13	0.73	0.58
$h_v$ [kW/m <sup>3</sup> ·K]	16.85	20.70	3.68	16.48	9.17	14.54

As shown in the table, ED is intrinsically dependent not only on material properties and dimensions, but also on the sensible contributions and thus temperature levels imposed on the unit, as seen in the results for Unit 2 at two temperature levels. With a similar point of view,  $\Phi_{PCM}$  shows a similar trend between the Units, but focusing only on the share of main energy storage material. Although it does not provide the exact same information, it can be useful in representing

both the compactness degree of the design, and the potential for energy density of the unit without considering the current experimental temperature differences.

On the heat transfer performance side, specific charging rate  $\gamma$  as proposed by Guo et al. [39], and 5 min peak power-energy stored ratio by Gasia et al. [38] seem to agree with the overall trend shown by NHTPC across the units. They provide indications of the average heat transfer behavior with respect to the total energy, but remain dependent on both temperature and HTF mass flow rate differences. In contrast, NHTPC remains almost constant for a given system across different experimental conditions.

Although they all provide very useful information on particular aspects, slightly more drastic variations can be seen with the volumetric heat transfer coefficient  $h_v$  and average temperature effectiveness  $\varepsilon_{avg}$  presented by Nomura et al. [40] as well as  $t_{Disch}$ ,  $\dot{Q}_{avg}$  and 5 min. Peak Power.

## 5. Conclusions

A pair of performance indicators to evaluate the heat transfer performance and compactness for latent heat energy storage (LHES) units were presented. These key performance indicators (KPIs) were calculated for several LHES units reported in literature allowing a leveled performance comparison with regard to operating conditions at different scales, while remaining intrinsic to the geometry, heat exchanger structure materials, and PCM. The robustness of the proposed KPIs was confirmed with varying HTF mass flow rate and temperature levels, for units at different size scales, with a coefficient of variance below 6% in every case, and were compared to other reported KPIs for LHES.

Finned tube bundle (FTB) and tube bundle (TB) units showed the widest range of performance, and a great potential mainly dependent on the quality of the HEX design. Composites in general require further experimental work but show very promising potential.

Automotive heat exchanger (AHEX)-based units showed promise especially on their heat transfer performance, and are interesting for further study as they are already mass produced in a very wide range of variations. Capillary tube bundles (CTBs) show great potential especially in terms of compactness, but due to the added practical challenges require some optimization work for ideal operation. For both AHEX and CTBs, material limitations regarding compatibility and operation range are some of the main concerns, and should be thoroughly considered in further studies.

The macro encapsulated (ME)-based systems considered showed in general low performance and compactness, but a very large potential for improvement and flexibility, especially in terms of capsule shape and size optimization to customize their performance, for instance.

It is necessary to highlight that the publications taken into account had clear application-oriented objectives. This implies that achieving the highest possible heat transfer rate was not the focus during their conception, but only the required performance for a specific application under given conditions. It is possible to infer that optimized versions of the mentioned technologies would deliver considerably higher performance indicators. Therefore, the conclusions drawn from this analysis cannot be considered as final in any way regarding the technological approaches but more so as a look at the general potential of each approach.

Additionally, a key aspect of the thermal response is relatively overlooked by the analysis, as the methodology proposed only accounts for the stability of the outlet temperature indirectly, within the approximation of the average outlet temperature. Further dimensionless analysis is required to account for this effect.

**Author Contributions:** Conceptualization, S.M. and R.W.; Formal analysis, W.D.-D.; Funding acquisition, A.S.; Investigation, W.D.-D.; Methodology, W.D.-D.; Project administration, W.D.-D. and A.S.; Resources, A.S.; Supervision, A.S. and J.W.; Writing—original draft, W.D.-D.; Writing—review and editing, A.S., S.M., R.W. and J.W. All authors have read and agreed to the published version of the manuscript.

**Funding:** This research was funded by the Swiss Competence Center for Energy Research Heat and Electricity Storage (SCCER HaE).

**Acknowledgments:** This work was developed within the framework of the Swiss Competence Center for Energy Research Storage of Heat and Electricity (SCCER HaE).

**Conflicts of Interest:** The authors declare no conflict of interest. The funders had no role in the design of the study; in the collection, analyses, or interpretation of data; in the writing of the manuscript, or in the decision to publish the results.

## Appendix A

**Table A1.** Additional information.

Type	$T_{init}$ [°C]	$\overline{T}_{HTF,In}$ [°C]	$\overline{T}_{HTF,Out}$ [°C]	HTF	PCM	$V_{PCM}$ [m <sup>3</sup> ]	HEX	Container	Ref.
TB (A.1)	68.0	15.0	33.85	Water	CH <sub>3</sub> COONa ·3H <sub>2</sub> O	$1.7 \times 10^{-2}$	Cu	PP	[7]
FTB (A.2)	68.0	16.0	48.65	Water	CH <sub>3</sub> COONa ·3H <sub>2</sub> O	$1.7 \times 10^{-2}$	Cu/Al	PP	[7]
TB (B.1)	55.0	20.0	20.02	Water	RT35	$7.1 \times 10^{-4}$	Cu	Methacrylate	[48]
FTB (B.2)	55.0	20.0	20.18	Water	RT35	$6.5 \times 10^{-4}$	Cu	Methacrylate	[48]
Triplex FTB(C)	92.0	68.0	69.09	Water	RT 82	$6.8 \times 10^{-3}$	Cu	Cu	[9]
FTB (D.1)	45.0	100.0	99.72	Water	Xylitol	$2.8 \times 10^{-3}$	Cu	No Info. Asm. Cu	[14]
FTB (E.1)	330.0	280.0	282.58	Thermal Oil	NaNO <sub>3</sub>	$1.7 \times 10^{-1}$	Steel/Al alloy	No Info. Asm. Steel	[10]
FTB (F)	162.0	122.0	134.32	Hi-Tech Therm 60	KNO <sub>3</sub> / NaNO/ NaNO <sub>2</sub>	$6.2 \times 10^{-2}$	Cu	SS304	[8]
FTB (G)	155.0	105.0	113.25	Marlotherm SH	HDPE	$2.6 \times 10^{-1}$	Steel / AlMg2.5	Steel	[47]
FTB (H)	72.0	20.0	44.12	Water	Organic	$2.9 \times 10^{-3}$	Al	Glass	[13]
FTB (I)	60.0	10.0	18.71	Water	RT44HC	$5.3 \times 10^{-2}$	Cu	Cu	[49]
FTB (J)	190.0	90.0	96.37	Hytherm 600	A164	$5.4 \times 10^{-3}$	SS316	SS316	[12]
Graphite matrix (B.3)	55.0	20.0	20.18	Water	RT35	$6.5 \times 10^{-4}$	Cu	Methacrylate	[48]
TB (K.1)	55.0	38.0	43.52	Water	Organic	$1.8 \times 10^{-2}$	Cu	No Info. Asm. Cu	[55]
Carbon brushes (K.2)	55.0	38.0	48.43	Water	Organic	$1.8 \times 10^{-2}$	Cu	No Info. Asm. Cu	[55]
Carbon cloth (L)	55.0	38.0	48.48	Water	Organic	$1.8 \times 10^{-2}$	Cu	No Info. Asm. Cu	[19]
Graphite matrix (M)	65.0	25.0	50.96	Water	Paraffin	$1.5 \times 10^{-2}$	Cu/Exp Graphite	None req.	[16]
TB (N.1)	70.0	25.0	36.51	Air	PCM 58P	$5.2 \times 10^{-4}$	Al / Foam	Al	[22]
MF 95% porosity (N.2)	70.0	25.0	47.23	Air	PCM 58P	$5.0 \times 10^{-4}$	Al / Foam	Al	[22]
MF 77% porosity (N.3)	70.0	25.0	47.18	Air	PCM 58P	$4.0 \times 10^{-4}$	Al /Foam	Al	[22]

Table A1. Cont.

Type	$T_{init}$ [°C]	$\overline{T_{HTF,In}}$ [°C]	$\overline{T_{HTF,Out}}$ [°C]	HTF	PCM	$V_{PCM}$ [m <sup>3</sup> ]	HEX	Container	Ref.
ME (O)	627.0	527.0	571.85	Air	Al-25 wt%-Si	$1.2 \times 10^{-3}$	AISI 316	AISI 316	[27]
ME (P)	535.0	380.0	416.06	Air	Na <sub>2</sub> SO <sub>4</sub> -KCl	$6.8 \times 10^{-3}$	Carbon steel	Carbon steel	[28]
ME (Q)	70.0	32.0	48.30	Water	Myristic Acid	$2.3 \times 10^{-2}$	HDPE	Steel	[30]
Pouch ME (R.1)	75.0	45.0	51.28	Water	1-Octa -decanol	$9.0 \times 10^{-2}$	Laminated PE, PA, Al, and PET	No Info. Asm. Steel	[31]
Sphere ME (R.2)	75.0	45.0	45.85	Water	1-Octa -decanol	$9.0 \times 10^{-2}$	Laminated PE, PA, Al, and PET	No Info. Asm. Steel	[31]
AHEX (B.4)	55.0	20.0	21.29	Water	RT35	$1.4 \times 10^{-3}$	Al/Cu	Methacrylate	[48]
AHEX (S)	3.5	24.0	17.08	Air	Organic	$1.8 \times 10^{-3}$	Al	No Info. Asm. Al	[50]
AHEX (T)	70.0	28.3	41.87	Water	Stearic Acid	$2.8 \times 10^{-3}$	Al	No Info. Asm. Al	[51]
AHEX (D.2)	45.0	100.0	99.83	90% Eth-Glycol	Xylitol	$1.3 \times 10^{-3}$	AL1100	No Info. Asm. Al	[14]
CTB (U)	30.0	25.0	28.63	Water	Organic	$9.7 \times 10^{-1}$	PP	No Info. Asm. PP	[52]
CTB (V)	33.0	22.0	24.58	Water	CaCl <sub>2</sub> · 6H <sub>2</sub> O	$8.0 \times 10^{-1}$	PP	PE	[53]
CTB (W)	35.0	22.0	25.75	Water	CaCl <sub>2</sub> · 6H <sub>2</sub> O	1.4	PP	PVC	[54]

## References

- Child, M.; Bogdanov, D.; Breyer, C. The role of storage technologies for the transition to a 100% renewable energy system in Europe. *Energy Procedia* **2018**, *155*, 44–60. [CrossRef]
- Prognos AG; Infrac AG; TEP Energy GmbH; Bundesamt für Energie. *Analyse des Schweizerischen Energieverbrauchs 2000–2017*; Federal Office for Energy: Bern, Switzerland, 2018.
- Heat Roadmap Europe. Heating and Cooling. Facts and Figures. The Transformation Towards a Low-carbon Heating & Cooling Sector. 2017. Available online: <https://heatroadmap.eu/heating-and-cooling-energy-demand-profiles/> (accessed on 3 May 2020).
- Benato, A.; Stoppato, A. Pumped Thermal Electricity Storage: A technology overview. *Therm. Sci. Eng. Prog.* **2018**, *6*, 301–315. [CrossRef]
- Miró, L.; Gasia, J.; Cabeza, L.F. Thermal energy storage (TES) for industrial waste heat (IWH) recovery: A review. *Appl. Energy* **2016**, *179*, 284–301. [CrossRef]
- Seddegh, S.; Wang, X.; Henderson, A.D. Numerical investigation of heat transfer mechanism in a vertical shell and tube latent heat energy storage system. *Appl. Therm. Eng.* **2015**, *87*, 698–706. [CrossRef]
- Waser, R.; Maranda, S.; Stamatiou, A.; Zaglio, M.; Worlitschek, J. Modeling of solidification including supercooling effects in a fin-tube heat exchanger based latent heat storage. *Sol. Energy* **2018**, 1–12. [CrossRef]
- Niyas, H.; Rao, C.R.C.; Muthukumar, P. Performance investigation of a lab-scale latent heat storage prototype—Experimental results. *Sol. Energy* **2017**, *155*, 971–984. [CrossRef]
- Al-Abidi, A.A.; Mat, S.; Sopian, K.; Sulaiman, M.Y.; Mohammad, A.T. Experimental study of melting and solidification of PCM in a triplex tube heat exchanger with fins. *Energy Build.* **2014**, *68*, 33–41. [CrossRef]
- Laing, D.; Bauer, T.; Breidenbach, N.; Hachmann, B.; Johnson, M. Development of high temperature phase-change-material storages. *Appl. Energy* **2013**, *109*, 497–504. [CrossRef]
- Johnson, M.; Vogel, J.; Hempel, M.; Hachmann, B.; Dengel, A. Design of high temperature thermal energy storage for high power levels. *Sustain. Cities Soc.* **2017**, *35*, 758–763. [CrossRef]
- Raul, A.K.; Bhavsar, P.; Saha, S.K. Experimental study on discharging performance of vertical multitube shell and tube latent heat thermal energy storage. *J. Energy Storage* **2018**, *20*, 279–288. [CrossRef]

13. Amagour, M.E.H.; Rachek, A.; Bennajah, M.; Ebn Touhami, M. Experimental investigation and comparative performance analysis of a compact finned-tube heat exchanger uniformly filled with a phase change material for thermal energy storage. *Energy Convers. Manag.* **2018**, *165*, 137–151. [[CrossRef](#)]
14. Shon, J.; Kim, H.; Lee, K. Improved heat storage rate for an automobile coolant waste heat recovery system using phase-change material in a fin-tube heat exchanger. *Appl. Energy* **2014**, *113*, 680–689. [[CrossRef](#)]
15. Xia, L.; Zhang, P.; Wang, R.Z. Preparation and thermal characterization of expanded graphite/paraffin composite phase change material. *Carbon* **2010**, *48*, 2538–2548. [[CrossRef](#)]
16. Wu, J.; Feng, Y.; Liu, C.; Li, H. Heat transfer characteristics of an expanded graphite/paraffin PCM-heat exchanger used in an instantaneous heat pump water heater. *Appl. Therm. Eng.* **2018**, *142*, 644–655. [[CrossRef](#)]
17. Nomura, T.; Tabuchi, K.; Zhu, C.; Sheng, N.; Wang, S.; Akiyama, T. High thermal conductivity phase change composite with percolating carbon fiber network. *Appl. Energy* **2015**, *154*, 678–685. [[CrossRef](#)]
18. Karthik, M.; Faik, A.; Blanco-Rodríguez, P.; Rodríguez-Aseguinolaza, J.; D’Aguanno, B. Preparation of erythritol–graphite foam phase change composite with enhanced thermal conductivity for thermal energy storage applications. *Carbon* **2015**, *94*, 266–276. [[CrossRef](#)]
19. Nakaso, K.; Teshima, H.; Yoshimura, A.; Nogami, S.; Hamada, Y.; Fukai, J. Extension of heat transfer area using carbon fiber cloths in latent heat thermal energy storage tanks. *Chem. Eng. Process. Process Intensif.* **2008**, *47*, 879–885. [[CrossRef](#)]
20. Xiao, M.; Feng, B.; Gong, K. Thermal performance of a high conductive shape-stabilized thermal storage material. *Sol. Energy Mater. Sol. Cells* **2001**, *69*, 293–296. [[CrossRef](#)]
21. Lazzarin, R.M.; Mancin, S.; Noro, M.; Righetti, G. Hybrid PCM-aluminium foams’ thermal storages: An experimental study. *Int. J. Low Carbon Technol.* **2018**, *13*, 286–291. [[CrossRef](#)]
22. Atal, A.; Wang, Y.; Harsha, M.; Sengupta, S. Effect of porosity of conducting matrix on a phase change energy storage device. *Int. J. Heat Mass Transf.* **2016**, *93*, 9–16. [[CrossRef](#)]
23. Mancin, S.; Diani, A.; Doretto, L.; Hooman, K.; Rossetto, L. Experimental analysis of phase change phenomenon of paraffin waxes embedded in copper foams. *Int. J. Therm. Sci.* **2015**, *90*, 79–89. [[CrossRef](#)]
24. Xiao, X.; Zhang, P.; Li, M. Effective thermal conductivity of open-cell metal foams impregnated with pure paraffin for latent heat storage. *Int. J. Therm. Sci.* **2014**, *81*, 94–105. [[CrossRef](#)]
25. Thapa, S.; Chukwu, S.; Khaliq, A.; Weiss, L. Fabrication and analysis of small-scale thermal energy storage with conductivity enhancement. *Energy Convers. Manag.* **2014**, *79*, 161–170. [[CrossRef](#)]
26. Oya, T.; Nomura, T.; Okinaka, N.; Akiyama, T. Phase change composite based on porous nickel and erythritol. *Appl. Therm. Eng.* **2012**, *40*, 373–377. [[CrossRef](#)]
27. Ma, F.; Zhang, P. Investigation on the performance of a high-temperature packed bed latent heat thermal energy storage system using Al-Si alloy. *Energy Convers. Manag.* **2017**, *150*, 500–514. [[CrossRef](#)]
28. Wickramaratne, C.; Moloney, F.; Pirasaci, T.; Kamal, R.; Goswami, D.; Stefanakos, E.; Dhau, J. Experimental Study on Thermal Storage Performance of Cylindrically Encapsulated PCM in a Cylindrical Storage Tank With Axial Flow. In Proceedings of the ASME 2016 Power Conference Collocated with the ASME 2016 10th International Conference on Energy Sustainability and the ASME 2016 14th International Conference on Fuel Cell Science, Engineering and Technology, Charlotte, NC, USA, 26–30 June 2016; p. V001T08A014. [[CrossRef](#)]
29. Pirasaci, T.; Wickramaratne, C.; Moloney, F.; Goswami, D.Y.; Stefanakos, E. Influence of design on performance of a latent heat storage system for a direct steam generation power plant. *Appl. Energy* **2018**, *224*, 220–229. [[CrossRef](#)]
30. Nallusamy, N.; Sampath, S.; Velraj, R. Experimental investigation on a combined sensible and latent heat storage system integrated with constant/varying (solar) heat sources. *Renew. Energy* **2007**, *32*, 1206–1227. [[CrossRef](#)]
31. Park, J.; Shin, D.H.; Lee, S.J.; Shin, Y.; Karng, S.W. Effective latent heat thermal energy storage system using thin flexible pouches. *Sustain. Cities Soc.* **2018**. [[CrossRef](#)]
32. Jesumathy, S.; Udayakumar, M.; Suresh, S. Experimental study of enhanced heat transfer by addition of CuO nanoparticle. *Heat Mass Transf. Und Stoffuebertragung* **2012**, *48*, 965–978. [[CrossRef](#)]
33. Harikrishnan, S.; Magesh, S.; Kalaiselvam, S. Preparation and thermal energy storage behaviour of stearic acid–TiO<sub>2</sub> nanofluids as a phase change material for solar heating systems. *Thermochim. Acta* **2013**, *565*, 137–145. [[CrossRef](#)]
34. Harikrishnan, S.; Imran Hussain, S.; Devaraju, A.; Sivasamy, P.; Kalaiselvam, S. Improved performance of a newly prepared nano-enhanced phase change material for solar energy storage. *J. Mech. Sci. Technol.* **2017**, *31*, 4903–4910. [[CrossRef](#)]

35. Romani, J.; Gasia, J.; Solé, A.; Takasu, H.; Kato, Y.; Cabeza, L.F. Evaluation of energy density as performance indicator for thermal energy storage at material and system levels. *Appl. Energy* **2019**, *235*, 954–962. [[CrossRef](#)]
36. Wang, W.W.; Wang, L.B.; He, Y.L. The energy efficiency ratio of heat storage in one shell-and-one tube phase change thermal energy storage unit. *Appl. Energy* **2015**, *138*, 169–182. [[CrossRef](#)]
37. Li, G. Energy and exergy performance assessments for latent heat thermal energy storage systems. *Renew. Sustain. Energy Rev.* **2015**, *51*, 926–954. [[CrossRef](#)]
38. Gasia, J.; Diriken, J.; Bourke, M.; Van Bael, J.; Cabeza, L.F. Comparative study of the thermal performance of four different shell-and-tube heat exchangers used as latent heat thermal energy storage systems. *Renew. Energy* **2017**, *114*, 934–944. [[CrossRef](#)]
39. Guo, X.; Goumba, A.P. Process intensification principles applied to thermal energy storage systems—A brief review. *Front. Energy Res.* **2018**, *6*, 1–10. [[CrossRef](#)]
40. Nomura, T.; Tsubota, M.; Oya, T.; Okinaka, N.; Akiyama, T. Heat release performance of direct-contact heat exchanger with erythritol as phase change material. *Appl. Therm. Eng.* **2013**, *61*, 28–35. [[CrossRef](#)]
41. Krimmel, S.; Stamatou, A.; Worlitschek, J.; Walter, H. Experimental characterization of the heat transfer in a latent direct contact thermal energy storage with one nozzle in labor scale. *Int. J. Mech. Eng.* **2018**, *3*, 83–97.
42. Incropera, F.P. *Fundamentals of Heat and Mass Transfer*; John Wiley and Sons, Inc.: Hoboken, NJ, USA, 2006.
43. Tay, N.H.; Belusko, M.; Bruno, F. An effectiveness-NTU technique for characterising tube-in-tank phase change thermal energy storage systems. *Appl. Energy* **2012**, *91*, 309–319. [[CrossRef](#)]
44. Tay, N.H.; Belusko, M.; Castell, A.; Cabeza, L.F.; Bruno, F. An effectiveness-NTU technique for characterising a finned tubes PCM system using a CFD model. *Appl. Energy* **2014**, *131*, 377–385. [[CrossRef](#)]
45. Incropera, F.; DeWitt, D.; Bergman, T.; Lavine, A. *Fundamentals of Heat and Mass Transfer*; Wiley: Hoboken, NJ, USA, 2007.
46. Mao, Q.; Liu, N.; Peng, L. Numerical Investigations on Charging / Discharging Performance of a Novel Truncated Cone Thermal Energy Storage Tank on a Concentrated Solar Power System. *Int. J. Photoenergy* **2019**, *2019*.
47. Zauner, C.; Hengstberger, F.; Etzel, M.; Lager, D.; Hofmann, R.; Walter, H. Experimental characterization and simulation of a fin-tube latent heat storage using high density polyethylene as PCM. *Appl. Energy* **2016**, *179*, 237–246. [[CrossRef](#)]
48. Medrano, M.; Yilmaz, M.O.; Nogués, M.; Martorell, I.; Roca, J.; Cabeza, L.F. Experimental evaluation of commercial heat exchangers for use as PCM thermal storage systems. *Appl. Energy* **2009**, *86*, 2047–2055. [[CrossRef](#)]
49. Khan, Z.; Khan, Z.A. An experimental investigation of discharge/solidification cycle of paraffin in novel shell and tube with longitudinal fins based latent heat storage system. *Energy Convers. Manag.* **2017**, *154*, 157–167. [[CrossRef](#)]
50. Lee, D.W. Experimental study on performance characteristics of cold storage heat exchanger for ISG vehicle. *Int. J. Automot. Technol.* **2017**, *18*, 41–48. [[CrossRef](#)]
51. Park, S.; Woo, S.; Shon, J.; Lee, K. Experimental study on heat storage system using phase-change material in a diesel engine. *Energy* **2017**, *119*, 1108–1118. [[CrossRef](#)]
52. Hejcik, J.; Charvat, P.; Klimes, L.; Astrouski, I. A Pcm-Water Heat Exchanger with Polymeric Hollow Fibres for Latent Heat Thermal Energy Storage: A Parametric Study of Discharging Stage. *J. Theor. Appl. Mech.* **2016**, *54*, 1285–1295. [[CrossRef](#)]
53. Helm, M.; Keil, C.; Hiebler, S.; Mehling, H.; Schweigler, C. Solar heating and cooling system with absorption chiller and low temperature latent heat storage: Energetic performance and operational experience. *Int. J. Refrig.* **2009**, *32*, 596–606. [[CrossRef](#)]
54. Helm, M.; Hagel, K.; Pfeiffer, W.; Hiebler, S.; Schweigler, C. Solar heating and cooling system with absorption chiller and latent heat storage—A research project summary. *Energy Procedia* **2014**, *48*, 837–849. [[CrossRef](#)]
55. Fukai, J.; Hamada, Y.; Morozumi, Y.; Miyatake, O. Improvement of thermal characteristics of latent heat thermal energy storage units using carbon-fiber brushes: Experiments and modeling. *Int. J. Heat Mass Transf.* **2003**, *46*, 4513–4525. [[CrossRef](#)]

